

Filamentary structure on the Sun from the magnetic Rayleigh–Taylor instability

Hiroaki Isobe¹, Takehiro Miyagoshi¹, Kazunari Shibata¹ & Takaaki Yokoyama²

¹Kwasan and Hida Observatories, Kyoto University, Yamashina, Kyoto 607-8471, Japan

²Department of Earth and Planetary Science, University of Tokyo, Hongo, Bunkyo-ku, Tokyo 113-0033, Japan

Magnetic flux emerges from the solar surface as dark filaments connecting small sunspots with opposite polarities^{1–3}. The regions around the dark filaments are often bright in X-rays and are associated with jets^{4–6}. This implies plasma heating and acceleration, which are important for coronal heating. Previous two-dimensional simulations of such regions showed that magnetic reconnection between the coronal magnetic field and the emerging flux produced X-ray jets and flares, but left unresolved the origin of filamentary structure and the intermittent nature of the heating. Here we report three-dimensional simulations of emerging flux showing that the filamentary structure arises spontaneously from the magnetic Rayleigh–Taylor instability^{7,8}, contrary to the previous view that the dark filaments are isolated bundles of magnetic field that rise from the photosphere carrying the dense gas^{9–11}. As a result of the magnetic Rayleigh–Taylor

instability, thin current sheets are formed in the emerging flux, and magnetic reconnection occurs between emerging flux and the pre-existing coronal field in a spatially intermittent way. This explains naturally the intermittent nature of coronal heating and the patchy brightenings in solar flares.

We performed three-dimensional magnetohydrodynamic simulations of solar emerging flux and its reconnection with pre-existing magnetic field in the corona, with the highest resolution ever achieved. The numerical code is basically the same as that used in our previous two-dimensional simulations^{10,12,13}, but extended to include variations in the third (y) direction. The simulation box is designed to model the upper convection zone (convectively unstable), photosphere/chromosphere (10^4 K), and corona (10^6 K). The box size is $0 < x < 48,000$, $0 < y < 15,000$, $-1,500 < z < 19,500$ (units are kilometres throughout), which is resolved by $800 \times 400 \times 620$ grid points; z is the vertical direction and $z = 0$ corresponds to the level of the photosphere. The initial state is hydrostatic. To simulate an emerging flux region (EFR), a horizontal magnetic flux sheet is placed in the convection zone. A small perturbation is then imposed on the flux sheet within a finite domain ($22,500 < x < 25,500$), to excite the Parker instability^{10,11}. The magnetic field in the corona is oblique and antiparallel to the flux sheet. The boundary conditions are: a rigid wall at the bottom, a free boundary at the top, and periodic at the x and y boundaries. Following previous studies of fast magnetic reconnection, we adopt an anomalous resistivity model because localized resistivity is necessary for fast reconnection to occur^{14,15}.

Figure 1 shows the three-dimensional visualization of the simulation result, showing the isosurface of magnetic field strength $|\mathbf{B}|$, temperature distributions at the y boundary, a set of representative

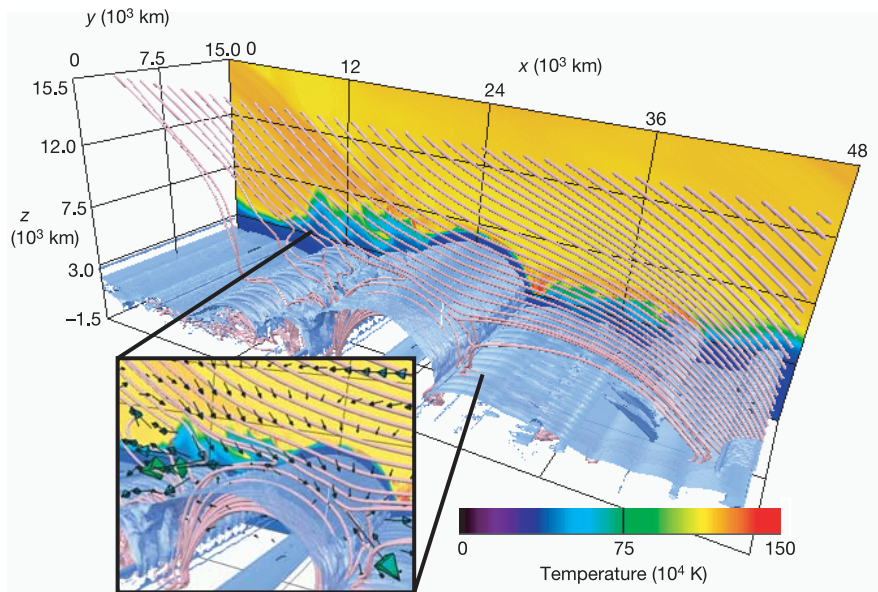


Figure 1 Three-dimensional visualization of the simulation result at $t = 2,500$ s. Isosurfaces of the magnetic field strength $|\mathbf{B}| = 40$ G (blue transparent surfaces), temperature distribution on a boundary (colour), and a set of magnetic field lines near $y = 2,400$ km (pink tubes) are shown. The simulation box contains the corona (10^6 K), the chromosphere/photosphere (10^4 K) and the convection zone (convectively unstable gas layer). The initial magnetic field of the flux sheet is given by: $\mathbf{B}_{\text{sheet}}(z) = (B_s(z), 0, 0)$ ($-1,200 < z < -600$). $B_s(z)$ is chosen so that the plasma β (the ratio of gas pressure to magnetic pressure) in the initial flux sheet is 4 in the range $-1,200 < z < -600$, $B_s(-600) \approx 1,200$ G and $B_s(-1,200) \approx 2,100$ G. We also impose a uniform oblique field that has a component antiparallel with the initial flux sheet: $\mathbf{B}_{\text{corona}} = (-B_c \cos \theta, 0, B_c \sin \theta)$, where $B_c = 26$ G and $\theta = 150^\circ$. The plasma β in the initial corona is about 2.6. The initial perturbation is imposed on the z component of the

velocity in the range $22,500 < x < 25,500$ and $-1,200 < z < -600$, $V_z = V_p \cos(2\pi(x - x_{\text{mid}})/\lambda)$, where $V_p = 0.5 \text{ km s}^{-1}$, $x_{\text{mid}} = 24,000$ km and $\lambda = 6,000$ km. When the emerging flux enters the corona, current sheets form near $(x, z) = (25,000, 7,000)$ where the emerging flux and coronal magnetic field is most antiparallel. The current sheet is recognized as the thin high-temperature (1.5×10^6 K) region. At this time the plasma β near the reconnection region is about 0.001 in the emerging flux and about 1 in the corona. The inset shows a close-up of the vicinity of magnetic reconnection region. The arrows indicate the velocity field. A pair of V-shaped field lines and oppositely directed plasma flows are the signature of magnetic reconnection. Although the morphology and dynamics do not vary significantly along the y direction, three-dimensional structure is seen in the isosurface of $|\mathbf{B}|$.

magnetic field lines, and the velocity field at $t = 2,500$ s. The omega-shaped structure seen in the $|\mathbf{B}|$ isosurfaces and field lines is the emerging flux. As the emerging flux pushes the coronal field, thin current concentrations with a high current density are formed near

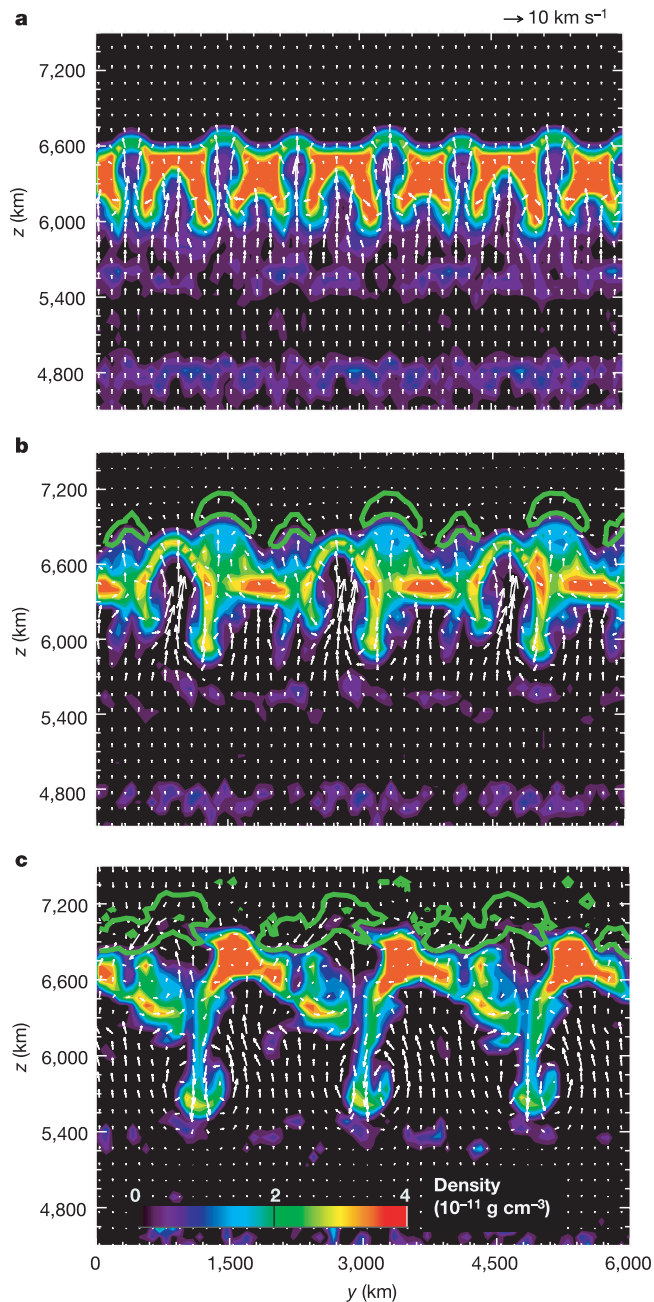


Figure 2 Temporal evolution of the mass density (colour), velocity (arrows) and resistivity (green contour) on a y - z plane near the reconnection points. The times are $t = 1,976$ s (**a**), $t = 2,028$ s (**b**) and $t = 2,106$ s (**c**), and the y - z plane is at $x = 24,400$ km. Only the velocity components on the plane (that is, the y and z components) are shown. The contour level of resistivity is $6 \times 10^{-11} \text{ cm}^2 \text{ s}^{-1}$, showing the region where anomalous resistivity sets in. The functional form of the resistivity is taken to be $\eta = \eta_0$ for $v_d < v_c$ and $\eta = \eta_0 + \eta_0 (v_d/v_c - 1)^2$ for $v_d > v_c$, where $v_d = J/\rho$ is the non-dimensional electron drift velocity, ρ is the mass density, J is the current density, and v_c is the threshold above which the anomalous resistivity sets in. The inclusion of constant background resistivity $\eta_0 = 3 \times 10^{-11} \text{ cm}^2 \text{ s}^{-1}$ is for numerical stability and does not significantly affect the dynamics of the emerging flux because the timescale of the slow reconnection/diffusion by the constant resistivity is much larger than the dynamical timescale of the emerging flux.

$(x, z) = (25,000, 7,000)$ and anomalous resistivity sets in there. Then fast reconnection of the magnetic field occurs, which is manifested by sets of highly bent field lines that, like stretched rubber bands, accelerate plasma in opposite directions (Fig. 1, inset).

The morphology and dynamics are similar in the y direction. More detail is given in previous two-dimensional work^{12,13}. However, note that the three-dimensional structure is seen in the isosurfaces of $|\mathbf{B}|$. Although no variation along the y direction is imposed explicitly in the initial conditions, there is numerical noise of the order of 10^{-7} or less, which grows nonlinearly and forms a three-dimensional structure. We found that the growth of the three-dimensional structure is due to the magnetic Rayleigh–Taylor instability^{7,8}. Figure 2 shows the mass density, velocity and resistivity distributions on the y - z plane at $x = 24,400$ km. The denser part near $z = 6,000$ – $7,000$ km corresponds to the top of the emerging flux. This top-heavy configuration is unstable for the Rayleigh–Taylor instability. As it grows through the nonlinear phase, the sinking spikes form mushroom-like structures due to the Kelvin–Helmholtz instability^{7,8}. Bending of the magnetic field, which is nearly perpendicular to the y - z plane, is stabilized by the magnetic tension. That is, only interchange modes grow. The resultant structure therefore consists of ‘filaments’ along the magnetic field.

A comparison with solar observations is given in Fig. 3. Figure 3a shows an H α image of an EFR. The arch filaments connect a small sunspot with a bright region covering a sunspot of the opposite polarity. The dark filaments correspond to cold ($\sim 10^4$ K) and dense ($\sim 10^{11} \text{ cm}^{-3}$) plasma. Figure 3b shows an extreme ultraviolet

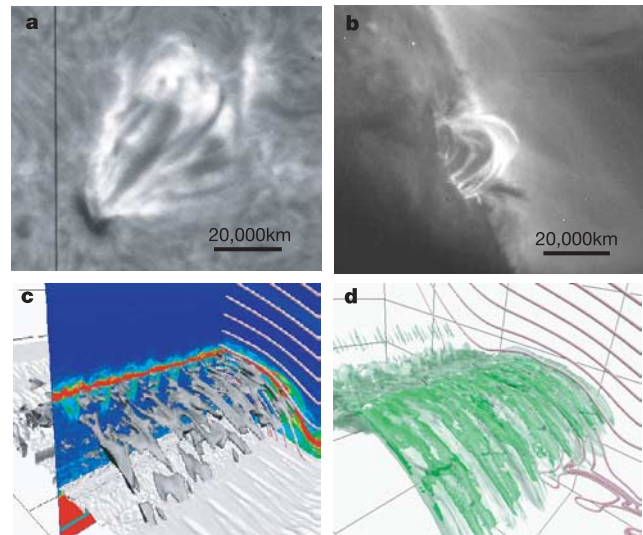


Figure 3 Comparison of the simulation result and observations. **a**, H α image of an EFR taken with the Domeless Solar Telescope at Hida observatory, Kyoto University, on 4 October 1991 (courtesy of H. Kurokawa and A. Edamura). The dark filaments connect a sunspot (lower left) with a bright region called plage (upper right). The length and width of the filaments are 10,000–30,000 km and 1,000–3,000 km, respectively. **b**, Extreme ultraviolet image of an EFR near the solar limb taken by the TRACE satellite on 8 June 1998. Bright loops are hot (10^6 K) and seen in emission, whereas dark loops are cold (10^4 K) and seen in absorption. A dark jet is being ejected from the lower side of the loops. **c**, Current density distribution on an x - z plane and a y - z plane (colour) as well as isosurfaces of mass density $\rho = 2 \times 10^{-11} \text{ g cm}^{-3}$ (grey surface) at $t = 2,200$ s. The isosurfaces of ρ trace the upper chromosphere and the dense filaments in the corona; $z > 4,000$ km is drawn in dark grey, to highlight the filaments in the corona. The red parts correspond to the strongest current region between the emerging flux and the coronal field. The green spikes below the red parts are the filamentary current sheets in the emerging flux itself, formed in the periphery of sinking spikes (mushrooms) as a result of the Rayleigh–Taylor instability. **d**, Isosurface of current density $6 \times 10^{-2} \text{ A m}^{-2}$ (green) and $6 \times 10^{-3} \text{ A m}^{-2}$ (transparent).

(EUV) image of another EFR near the solar limb. Bright loops are hot ($\sim 10^6$ K) and dark loops are cold ($\sim 10^4$ K). The coexistence of many hot and cold loops is evidence for spatially intermittent heating. Jets are ejected from the lower footpoints of the loops, indicating the occurrence of magnetic reconnection between the emerging flux and the pre-existing coronal field^{12,13,16}.

The grey surfaces in Fig. 3c are isosurfaces of mass density in the simulation. The dark grey surfaces trace the cold and dense plasma in the corona. They appear as isolated filaments that are very similar to the observed dark filaments. The colours on the vertical planes are the current density distributions; they show many small current sheets created in the emerging flux by the Rayleigh–Taylor instability. Dissipation of the filamentary current sheets leads to heating of the plasma in the periphery of the dense filaments and formation of a system of hot and cold loops existing alternately. Thus, the intermittent heating of the emerging flux indicated by the EUV observations is explained naturally.

Observational evidence of the formation of current sheets in emerging flux has recently been reported¹⁷, supporting the idea that the corona is heated by dissipation of current sheets¹⁸. Shuffling of magnetic field by photospheric flows is often considered to be the driving mechanism of current formation in the corona^{18–20}. Our numerical simulations indicate that the Rayleigh–Taylor instability can also form current sheets in EFRs, and can also explain why the heating occurs in an intermittent way.

Such structure formation by the Rayleigh–Taylor and Kelvin–Helmholtz instabilities occurs in diverse situations in natural phenomena such as supernova remnants²¹ and technological applications such as laboratory laser implosion⁷. As for the origin of the arch filaments in the solar EFR, it is also possible that the emerging flux is already fragmented in the photosphere by, for example, turbulent convection. Even so, however, when the fragmented magnetic flux emerges into the upper atmosphere, magnetic energy becomes dominant and hence the fragmented magnetic flux tubes

expand horizontally and fill the space between them, developing the almost two-dimensional structure except at the edge of an EFR¹¹. Therefore, basically the same physical processes should occur in more complicated three-dimensional structures.

The formation of filamentary structure has significant consequences for the behaviour of magnetic reconnection. The green lines in Fig. 2 show resistivity contours. As the Rayleigh–Taylor instability grows through the nonlinear phase, the current density is enhanced in the rising part by upward forcing. Because the mass density is lower in the rising parts, the resistivity is locally enhanced in those parts owing to the anomalous resistivity model (see the legend to Fig. 2). Fast reconnection therefore starts only in the rising parts; the plasma is then accelerated and ejected from the current sheet by the reconnected magnetic field. The mass density and gas pressure in the diffusion region decrease, inducing plasma flows towards the diffusion region that pinch the current sheet. The current density and hence resistivity are thereby enhanced. It is a kind of nonlinear instability, known as spontaneous fast reconnection^{14,22}. In the present simulation, fast reconnection is initiated locally by the Rayleigh–Taylor instability, and the fast reconnection enhances the growth of the instability by inducing plasma flows. Therefore the Rayleigh–Taylor instability and the fast magnetic reconnection are nonlinearly coupled, resulting in spatially intermittent, ‘patchy’ reconnection.

Figure 4 shows the isosurfaces of velocity $|V|$ that trace the fast outflows from the reconnecting current sheets and also plasma flows moving upwards along the ambient field lines. Because of intermittent reconnection, many distinctive narrow outflows (jets) are identified. Although the present simulation cannot reproduce the electromagnetic radiation qualitatively, the patchy reconnection should produce patchy brightenings, which are actually observed in EFRs (see Fig. 3).

The intermittent, filamentary structures and patchy brightenings are often observed not only in EFRs but also in various solar phenomena^{23–25}. Considering the ubiquity of the filamentary/patchy structures, it is likely that, if the reconnecting current sheet is not in mechanical equilibrium and the densities of both the sides are different, patchy reconnection can occur by the coupling of anomalous resistivity with the Rayleigh–Taylor instability, as demonstrated in our high-resolution simulation. We conjecture that the same mechanism can be applied to explain the origin of filamentary structure and patchy brightenings in various dynamic phenomena in astrophysical, space and laboratory plasmas. \square

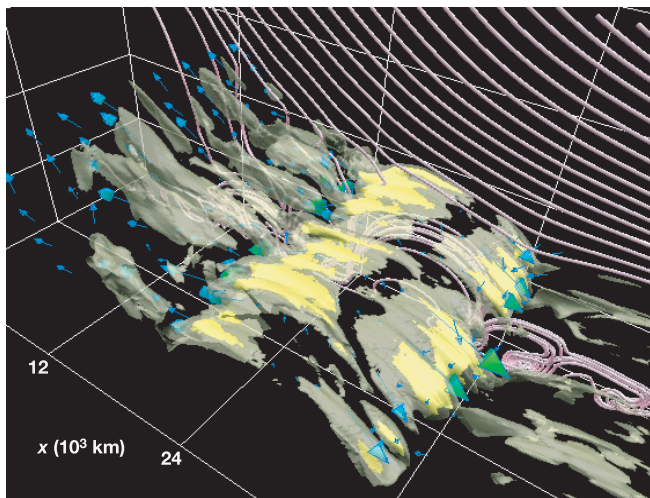


Figure 4 Three-dimensional visualization of the simulation result, showing the structure of plasma flows from reconnection points. The isosurfaces of velocity $|V| = 120 \text{ km}^{-1}$ (yellow) and 60 km^{-1} (transparent), velocity vector (arrows), and a set of field lines are shown. The isosurface of $|V| = 120 \text{ km}^{-1}$ traces the fast outflows ejected from reconnecting current sheets, whereas the $|V| = 60 \text{ km}^{-1}$ surface traces the jets moving upwards along the ambient field lines. Because of the patchy distribution of the reconnection points, many narrow jets are ejected from the current sheet. This may correspond to the fine structures observed in coronal jets. Although the present simulation cannot quantitatively reproduce the electromagnetic radiation observed, impulsive heating by the patchy reconnection should produce patchy brightenings in the chromosphere, the transition region and the corona because energy transport from the reconnection site by thermal conduction and high energy particles are only along the magnetic field.

Received 3 September 2004; accepted 26 January 2005; doi:10.1038/nature03399.

1. Bruzek, A. On arch-filament system in spotgroups. *Sol. Phys.* **2**, 451–461 (1967).
2. Zirin, H. Fine structure of solar magnetic fields. *Sol. Phys.* **22**, 34–48 (1972).
3. Frazier, E. N. The magnetic structure of arch filament system. *Sol. Phys.* **26**, 130–141 (1972).
4. Golub, L., Rosner, R., Vaiana, G. S. & Weiss, N. O. Solar magnetic fields: the generation of emerging flux. *Astrophys. J.* **243**, 309–316 (1981).
5. Yoshimura, K. & Kurokawa, H. Causal relations between H α loop emergences and soft X-ray brightenings. *Astrophys. J.* **517**, 964–976 (1999).
6. Shibata, K. *et al.* Observations of X-ray jets with the YOHKOH Soft X-ray Telescope. *Publ. Astron. Soc. Jpn.* **44**, L173–L179 (1992).
7. Sharp, D. H. An overview of Rayleigh–Taylor instability. *Physica* **12D**, 3–18 (1984).
8. Cattaneo, F. & Hughes, D. H. The nonlinear break up of a magnetic layer: instability to interchange modes. *J. Fluid Mech.* **196**, 323–344 (1988).
9. Zwaan, C. The emergence of magnetic flux. *Sol. Phys.* **100**, 397–414 (1985).
10. Shibata, K. *et al.* Nonlinear Parker instability of isolated magnetic flux in a plasma. *Astrophys. J.* **338**, 471–492 (1989).
11. Matsumoto, R., Tajima, T., Shibata, K. & Kaisig, M. Three-dimensional magnetohydrodynamics of the emerging magnetic flux in the solar atmosphere. *Astrophys. J.* **414**, 357–371 (1993).
12. Yokoyama, T. & Shibata, K. Magnetic reconnection as the origin of X-ray jets and H-alpha surges in the Sun. *Nature* **375**, 42–44 (1995).
13. Yokoyama, T. & Shibata, K. Numerical simulation of solar coronal X-ray jets based on the magnetic reconnection model. *Publ. Astron. Soc. Jpn.* **48**, 353–376 (1996).
14. Ugai, M. Computer studies on development of the fast reconnection mechanism for different resistivity models. *Phys. Fluids B* **4**, 2953–2963 (1992).
15. Yokoyama, T. & Shibata, K. What is the condition for fast magnetic reconnection? *Astrophys. J.* **436**, L197–L200 (1994).
16. Miyagoshi, T. & Yokoyama, T. Magnetohydrodynamic numerical simulations of solar X-ray jets based on the magnetic reconnection model that includes chromospheric evaporation. *Astrophys. J.* **593**, L133–L136 (2003).

17. Solanki, S. K. *et al.* Three-dimensional magnetic field topology in a region of solar coronal heating. *Nature* **425**, 692–695 (2003).
18. Parker, E. N. Nanoflare and the solar X-ray corona. *Astrophys. J.* **330**, 474–479 (1988).
19. Galsgaard, K. & Nordlund, A. Heating and activity of the solar corona. 1. Boundary shearing of an initially homogeneous magnetic field. *J. Geophys. Res.* **101**, 13445–13460 (1996).
20. Karpen, J. T., Antiochos, S. K. & DeVore, C. R. Reconnection-driven current filamentation in solar arcades. *Astrophys. J.* **460**, L73–L76 (1996).
21. Hachisu, I., Matsuda, T., Nomoto, K. & Shigeyama, T. Nonlinear growth of Rayleigh–Taylor instabilities and mixing in SN 1987A. *Astrophys. J.* **358**, L57–L61 (1990).
22. Ugai, M. & Shimizu, T. Computer studies on the spontaneous fast reconnection mechanism in three dimensions. *Phys. Plasmas* **3**, 853–862 (1996).
23. Kitahara, T. & Kurokawa, H. High-resolution observation and detailed photometry of a great H α two-ribbon flare. *Sol. Phys.* **125**, 321–332 (1990).
24. Innes, D. E., McKenzie, D. E. & Wang, T. SUMER spectral observations of post-flare supra-arcade inflows. *Sol. Phys.* **217**, 247–265 (2003).
25. Asai, A., Yokoyama, T., Shimojo, M. & Shibata, K. Downflow motions associated with impulsive nonthermal emissions observed in the 2002 July 23 solar flare. *Astrophys. J.* **605**, L77–L80 (2004).

Acknowledgements The authors thank N. O. Weiss, A. Asai and D. H. Brooks for comments. Use of TRACE data is acknowledged. This work was supported by the Japan–UK Cooperation Science Program of the JSPS (Principal investigators K.S. and N. O. Weiss) and a Grant-in-Aid for the 21st Century COE ‘Centre for Diversity and Universality in Physics’ from MEXT, Japan. The numerical computation was performed on the Earth Simulator.

Competing interests statement The authors declare that they have no competing financial interests.

Correspondence and requests for materials should be addressed to H.I. (isobe@kwasan.kyoto-u.ac.jp).

Spatial quantum noise interferometry in expanding ultracold atom clouds

Simon Fölling, Fabrice Gerbier, Artur Widera, Olaf Mandel, Tatjana Gericke & Immanuel Bloch

Institut für Physik, Johannes Gutenberg-Universität, Staudingerweg 7, D-55099 Mainz, Germany

In a pioneering experiment¹, Hanbury Brown and Twiss (HBT) demonstrated that noise correlations could be used to probe the properties of a (bosonic) particle source through quantum statistics; the effect relies on quantum interference between possible detection paths for two indistinguishable particles. HBT correlations—together with their fermionic counterparts^{2–4}—find numerous applications, ranging from quantum optics⁵ to nuclear and elementary particle physics⁶. Spatial HBT interferometry has been suggested⁷ as a means to probe hidden order in strongly correlated phases of ultracold atoms. Here we report such a measurement on the Mott insulator^{8–10} phase of a rubidium Bose gas as it is released from an optical lattice trap. We show that strong periodic quantum correlations exist between density fluctuations in the expanding atom cloud. These spatial correlations reflect the underlying ordering in the lattice, and find a natural interpretation in terms of a multiple-wave HBT interference effect. The method should provide a useful tool for identifying complex quantum phases of ultracold bosonic and fermionic atoms^{11–15}.

Although quantum noise correlation analysis is now a basic tool in various areas of physics, applications to the field of cold atoms have been scarce. Most of these concentrate on photon correlation techniques from quantum optics^{5,16}. It was not until 1996 that bunching of cold (but non-degenerate) bosonic atom clouds could be directly measured¹⁷, followed by the observation of reduced inelastic losses due to a modification of local few-body correlations by quantum degeneracy^{18–20}.

In our experiment, we directly measure the spatial correlation function of the density fluctuations in a freely expanding atomic

cloud^{7,21–23}. We create an ultracold Bose gas in an optical lattice with several hundred thousand occupied lattice sites, and record the density distribution after sudden switch-off of the trapping potential and a fixed period of free expansion (the ‘time of flight’). Resonant absorption of a probe laser²⁴ yields the two-dimensional column density of the cloud, that is, the density profile integrated along the probe line of sight, as illustrated in Fig. 1a. It should be noted that the density after the time of flight reflects the in-trap momentum distribution rather than the in-trap density distribution. We performed the experiment with a Bose gas initially in the Mott insulator regime^{8–10}, where repulsive interactions pin the atomic density to exactly an integer number of atoms per lattice site, typically between one and three. In this Mott insulator phase, the average density distribution after expansion is simply given by the

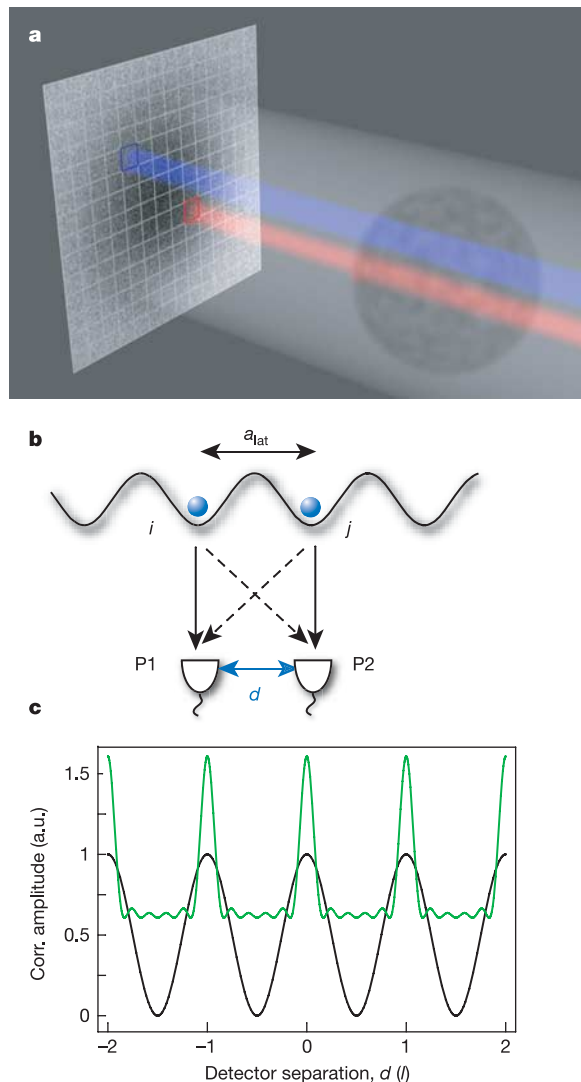


Figure 1 Illustration of the atom detection scheme and the origin of quantum correlations. **a**, The cloud of atoms is imaged to a detector plane and sampled by the pixels of a CCD camera. Two pixels P1 and P2 are highlighted, each of which registers the atoms in a column along its line of sight. Depending on their spatial separation d , their signals show correlated quantum fluctuations, as illustrated in **b**. **b**, When two atoms initially trapped at lattice sites i and j (separated by the lattice spacing a_{lat}) are released and detected independently at P1 and P2, the two indistinguishable quantum mechanical paths, illustrated as solid and dashed lines, interfere constructively for bosons (or destructively for fermions). **c**, The resulting joint detection probability (correlation amplitude) of simultaneously finding an atom at each detector is modulated sinusoidally as a function of d (black curve). The multiple wave generalization to a regular array of six sources with the same spacing is shown in green. a.u., arbitrary units.